Alterations in the Cerebral Microvascular Proteome Expression Profile After Transient Global Cerebral Ischemia in Rat

Spray, Stine; Johansson, Sara E; Edwards, Alistair; Larsen, Martin Røssel; Radziwon-Balicka, Aneta; Povlsen, Gro Klitgaard; Edvinsson, Lars

Published in:
Journal of Molecular Neuroscience

DOI:
10.1007/s12031-016-0875-8

Publication date:
2017

Document version
Publisher's PDF, also known as Version of record

Citation for pulished version (APA):
Spray, S., Johansson, S. E., Edwards, A. V. G., Larsen, M. R., Radziwon-Balicka, A., Povlsen, G. K., & Edvinsson, L. (2017). Alterations in the Cerebral Microvascular Proteome Expression Profile After Transient Global Cerebral Ischemia in Rat. Journal of Molecular Neuroscience, 61(3), 396–411. DOI: 10.1007/s12031-016-0875-8

J Mol Neurosci (2017) 61:396–411
DOI 10.1007/s12031-016-0875-8

Alterations in the Cerebral Microvascular Proteome Expression Profile After Transient Global Cerebral Ischemia in Rat

Stine Spray[1] · Sara E. Johansson[1] · Alistair V. G. Edwards[2] · Martin R. Larsen[2] · Aneta Radziwon-Balicka[1] · Gro K. Povlsen[1] · Lars Edvinsson[1,3]

Received: 19 October 2016 / Accepted: 29 November 2016 / Published online: 8 December 2016

Abstract This study aimed at obtaining an in-depth mapping of expressional changes of the cerebral microvasculature after transient global cerebral ischemia (GCI) and the impact on these GCI-induced expressional changes of post-GCI treatment with a mitogen-activated protein kinase kinase (MEK1/2) inhibitor. GCI was induced in male Wistar rats followed by treatment with either vehicle or the MEK1/2 inhibitor U0126 every 12 h post-GCI. Seventy-two hours after GCI or sham surgery, the cerebral microvasculature was isolated and the protein content analysed with state-of-the-art mass spectrometry. The proteomic profile of the isolated cerebral microvasculature 72 h after GCI (compared to sham) indicated that the main expressional changes could be divided into nine categories: (1) cellular respiration, (2) remodelling of the extracellular matrix, (3) decreased contractile phenotype, (4) clathrin-mediated endocytosis, (5) ribosomal activity, (6) expression of chromatin structure-related proteins, (7) altered synaptic activity, (8) altered G-protein signalling and (9) instability of the membrane potential. Treatment with U0126 partly normalized the expression of one or more of the proteins in all nine categories. Flow cytometry confirmed key findings from the proteome such as upregulation of the extracellular proteins lamininβ2 and nidogen2 ($p < 0.05$) after GCI. These results provide valuable molecular insight into the broad and complex expressional changes in the cerebral microvasculature after GCI and the effect of early MEK1/2 inhibitor treatment on these changes.

Keywords Cerebral microvasculature · Extracellular matrix remodelling · Global cerebral ischemia · MEK1/2 inhibitor treatment · Proteomics

Introduction

The cerebral vasculature is highly specialized to ensure a stable environment in the central nervous system with a continuous and constantly adapting cerebral blood flow (CBF). Half of the cerebral vascular resistance determining CBF resides in the extra-parenchymal arteries on the brain surface, which regulate input blood supply to the cerebral parenchyma. The other half of the cerebral resistance resides in the intraparenchymal microvasculature, which regulates the local CBF to meet the changing metabolic demands of active brain regions by a complex interplay of neurons, astrocytes and the intraparenchymal vasculature (Edvinsson and Krause 2002; Attwell et al. 2010).

Global cerebral ischemia (GCI) was previously shown to cause pathophysiological changes in the extra-parenchymal vasculature 48 and 72 h after the insult. Increased expression of contractile endothelin B (ET_B) and 5-hydroxytryptamine 1B ($5\text{-}HT_{1B}$) receptors and the calcium channel transient receptor potential canonical 1 and 6 in the vascular smooth muscle cells (VSMCs) of the large extra-parenchymal arteries correlated with a decrease in forebrain blood flow (Johansson et al. 2012, 2014, 2015). The increased contractility of the

Electronic supplementary material The online version of this article (doi:10.1007/s12031-016-0875-8) contains supplementary material, which is available to authorized users.

✉ Stine Spray
stine.spray@regionh.dk

[1] Department of Clinical Experimental Research, Glostrup Research Institute, Rigshospitalet, Glostrup, Denmark

[2] Department of Biochemistry and Molecular Biology, University of Southern Denmark, Odense, Denmark

[3] Department of Clinical Sciences, Division of Experimental Vascular Research, Lund University, Lund, Sweden

extra-parenchymal arteries is thought to contribute to the development of delayed neurological damage found in the days after GCI via decreased CBF (Edvinsson and Povlsen 2011; Johansson et al. 2012, 2014, 2015). Delayed neurological damage is a pathological event found in the brain 2–7 days after the initial episode of transient GCI where neurons in selective vulnerable areas succumb and die. The brain regions affected depend on the severity and length of the episode of transient GCI, and delayed neurological damage has been found in the hippocampus, caudate putamen, thalamus, cerebellum and cerebral cortex (Neumann et al. 2013; Petito et al. 1987; Pulsinelli et al. 1982; Zeng and Xu 2000). Delayed neurological damage causes delayed neurological deterioration and mortality in patients, and finding a treatment strategy that could prevent this delayed deterioration would improve the outcome and save many lives.

We have previously shown that treatment with a mitogen-activated kinase kinase (MEK1/2) inhibitor after GCI prevented upregulation of contractile receptors in the extra-parenchymal arteries and more importantly decreased delayed neurological damage, prevented the development of delayed mortality and improved overall well-being of the rats treated (Johansson et al. 2014). Furthermore, MEK1/2 activation has been shown to be involved in the activation of metalloproteinases and proinflammatory molecules causing blood-brain barrier (BBB) breakdown and inflammation, thereby worsening cerebral ischemic damage (Edvinsson and Povlsen 2011). Our overall hypothesis is that inhibiting the broad MEK1/2 signalling pathway transiently after cerebral ischemia and GCI prevents multiple damaging cellular processes in the extra-parenchymal vasculature, and this novel treatment approach targeting multiple processes will improve overall outcome in patients suffering from cerebral ischemia and GCI (Edvinsson and Povlsen 2011). In addition to preventing pathological changes in the extra-parenchymal vasculature, it seems likely that this treatment strategy may also prevent delayed pathological changes in the intraparenchymal cerebral vasculature and brain parenchyma (neurons and glial cells). Therefore, MEK1/2 inhibition is an exciting novel treatment strategy for delayed neurological complications after transient GCI. Currently, we have extensive knowledge of the effect of MEK1/2 inhibition on extra-parenchymal vascular changes, but the effect of MEK1/2 inhibition on microvascular changes after GCI is largely unknown. In this study, we investigated the GCI-induced changes of the cerebral intraparenchymal microvasculature and the effect of treatment with a MEK1/2 inhibitor post-GCI on these microvascular changes 72 h after GCI induction in a proteome study, since we have previously shown that at 72 h post-GCI, maximal contractile receptor contractility of the extra-parenchymal vasculature is occurring and neuronal cell death is starting to appear (Johansson et al. 2014).

The effects of GCI on the cerebral microvasculature are largely unknown and may contribute to the development of delayed neurological damage along with the changes in the large extra-parenchymal arteries after GCI. The intraparenchymal vasculature is an integrated part of the brain parenchyma whose local contractile state is primarily regulated by factors released by local astrocytes and neurons (Attwell et al. 2010). Another important feature of the cerebral microvasculature is that it constitutes a part of the BBB whose key role is protecting the vulnerable neurons from toxic compounds in the blood and creating a specialized environment for energy-efficient coordinated neuronal function and processing (Bradbury 1993). Due to these specialized characteristics of the intraparenchymal vasculature distinguishing it from the extra-parenchymal vasculature, it is highly relevant to investigate GCI-induced changes in the cerebral microvasculature.

Large-scale proteomics using advanced mass spectrometry allows precise in-depth mapping of relative but quantitative expressional changes in a given tissue at a given time point (Steen and Mann 2004). This technique is a valuable tool when examining the effects of a disease on a specific tissue or cell type and the effect of new treatments on these tissue-specific expressional changes. In this study, we performed a proteomic screen of the isolated cerebral microvasculature that enabled us to obtain a global map of expressional changes after GCI compared to sham-operated animals as well as the effect of treatment with a MEK1/2 inhibitor on these GCI-induced expressional changes.

Materials and Methods

Experimental Global Cerebral Ischemia in Rats

Male Wistar rats (9–11 weeks, 290–350 g, Taconic, Denmark) were used for the experiments, and they were provided with standard rat chow and water and were housed under 12-h light/dark cycle conditions. All animal experiments were carried out in accordance with EU guidelines (directive 2010/63/EU on the protection of animals used for scientific purposes) and the experimental protocol was approved by the Danish Experimental Animal Inspectorate (licence no. 2012-15-2934-00726).

Transient GCI was induced in male rats by occluding the common carotid arteries combined with systemic hypotension, which disrupts the blood flow to the forebrain (Johansson et al. 2012; Smith et al. 1984) resulting in forebrain ischemia. The rat was anaesthetized with 4% isoflurane in a mixture of O_2 and N_2O (30:70), intubated and supplied with 2% isoflurane during the surgery. The tail artery was cannulated for measurement of mean arterial blood pressure (MABP) and a tail vein cannulated for the administration of the muscle relaxant Norcuron (1.3 mL/h, Nomeco, Denmark). The MABP was lowered to 35–40 mmHg by withdrawing

blood from the jugular vein followed by clamping of the common carotid arteries for 15 min. During the entire procedure, body and scalp temperature at 37 ± 0.5 °C was ensured by thermometers in the rectum and subcutaneously above the scalp. Analgesics (Rimadyl®, Carprofen 5 mg/kg, Nomeco, Denmark) were supplied during surgery and again daily until euthanasia. The rats were housed individually 72 h after the surgery and euthanized by sedation in a mixture of CO_2 and O_2 followed by decapitation.

Experimental Groups and Treatment Protocol

A total of 30 rats were included in this study: 18 rats for the proteomics screen and 12 rats for flow cytometry. The rats for the proteomic screen were divided into three groups: (1) sham-operated treated with vehicle (500 μL DMSO, Sigma-Aldrich, Denmark), (2) GCI treated with vehicle and (3) GCI treated with the MEK1/2 inhibitor U0126 (30 mg/kg in 500 μL DMSO, LC Laboratories, USA). Treatment was allocated in a randomized fashion before the operations and given intraperitoneally at 0, 12, 24, 36, 48 and 60 h after sham or GCI induction. Seventy-two hours after the surgery, the animals were euthanized and the brains snap-frozen in ice-cold 2-methylbutane (Sigma-Aldrich) and stored at −80 °C until microvessel purification for the proteomic screen (Pardridge et al. 1987). For flow cytometry analysis, single-cell suspension with intraparenchymal microvasculature was isolated from the brains immediately after euthanasia 72 h after GCI (six rats) or sham (six rats) operation. Physiological data from different groups of animals were tested statistically by one-way ANOVA with Bonferroni's post test, and $p < 0.05$ was accepted as statistical significant.

Isolation of the Cerebral Microvasculature for the Proteomic Screen

The microvasculature of the six brains in each of the three treatment groups (sham with vehicle, GCI with vehicle and GCI with U0126) were purified separately but on the same day, respectively. Furthermore, individual brains within a group remained separate during preparation of the vascular fraction. The brains were thawed on ice followed by removal of extra-parenchymal vasculature and striatal brain structures in ice-cold physiological buffer solution 1 (PBS1) with the following composition: 138 mM NaCl, 10 mM HEPES, 4 mM KCl and 2.2 mM $CaCl_2$. The isolated cortical structures were gently homogenized in ice-cold PBS1, and the homogenate was centrifuged at 800×*g* for 5 min at 4 °C. The supernatant was discarded, and the pellet was resuspended in 10 mL of PBS1 with 15% dextran (MW range 64,000 to 74, 000, Sigma-Aldrich) and centrifuged at 20,000×*g* for 10 min at 4 °C. This resulted in a separation of the vasculature (pellet) and the neuronal/glial tissue (cholesterol-rich layer on top of the dextran solution). The pellet was resuspended in 10 mL of PBS1 with 15% dextran and subjected to a second round of centrifugation at 20,000×*g*. The pellet of enriched microvasculature was then resuspended in PBS1, transferred to a 40-μm cell strainer (Falcon, Corning®, VWR, Denmark) and washed with 10 mL of PBS1. The vascular structures retained on the filter were transferred to an Eppendorf tube, and 400 μL of prewarmed enzyme mixture (0.2% collagenase/dispase (Roche, Switzerland), 0.013% elastase (Sigma-Aldrich) and 2% BSA (Sigma-Aldrich)) was added followed by incubation at 37 °C for 15 min with frequent pipetting. The enzymatic activity was terminated by adding 4 mL of ice-cold Dulbecco's modified medium (Gibco, Life Technologies, Denmark) with 20% foetal bovine serum (Thermo Fischer Scientific, USA) to the samples, and the vascular structures were washed on a 40-μm cell strainer. The sample of the microvasculature retained on the cell strainer was collected by forceps, snap-frozen in an Eppendorf tube on dry ice and stored at −80 °C until protein purification. The samples were blinded prior to protein purification and mass spectrometry analysis.

Protein Purification, Peptide Preparation and Fractionation for Mass Spectrometry

The samples of cerebral intraparenchymal vasculature were dounce-homogenized in 0.1 M Na_2CO_3 (ice-cold) containing protease and phosphatase inhibitors (Roche, Meylan, France) and then sonicated for 2 × 20 s on ice. Homogenates were ultra-centrifuged at 150,000×*g* for 1.5 h. Pellets (membrane fractions) were resuspended in 6 M urea/2 M thiourea, supernatants (soluble fractions) were precipitated using 20% trichloroacetic acid, and pellets from this precipitation were resuspended in 6 M urea/2 M thiourea. All samples were reduced in 10 mM dithiothreitol and then alkylated using 20 mM iodoacetamide. Lysyl endopeptidase (Wako, Osaka, Japan) was added for 3 h followed by sixfold sample dilution in 50 mM triethylammonium bicarbonate. Trypsin (Promega, Madison, WI, USA) was added at a ratio of 1:40 (*w*/*w*) and left for 18 h to digest. Digests were acidified with formic acid (2% final concentration), and the protein content of aliquots was quantified using amino acid analysis. Maximum equal amounts of protein from each sample were labelled with iTRAQ four-plex reagent according to the manufacturer's instructions (AB Sciex, MA, USA), and equal labelling was confirmed on a Bruker UltraFlex MALDI MS (Bruker, MA, USA), and the three sample groups (sham with vehicle, GCI with vehicle and GCI with U0126) were combined to give equal reporter intensity.

Combined peptide samples were then enriched with titanium dioxide for isolation of glycosylated peptides. Briefly, the samples were incubated with titanium dioxide at a ratio of 0.6 mg Tio_2/100 μg peptide, in 80% acetonitrile (ACN), 5%

trifluroacetic acid (TFA) and 1 M glycolic acid. Flow through from this incubation became the 'non-modified' fraction, one with membrane peptides and one with cytosolic peptides. After incubation (10 min), TiO_2 beads were washed sequentially with 80% ACN/5% TFA, 80% ACN/0.1% TFA and 20% ACN/0.1% TFA. The peptides were eluted from titanium using 25% ammonia water (pH 11; Sigma). These became the titanium dioxide elution fractions. All peptide samples were cleaned up separately on homemade R3 columns (PerSeptive Biosystems, Framingham, MA, USA) and then dried down for hydrophilic interaction chromatography (HILIC). Peptide samples were resuspended in 90% ACN/0.1% TFA and loaded onto a micro-HILIC chromatography system. HILIC resin was TSK-Gel Amide 80 (Tosoh Bioscience, Japan). The samples were separated over a gradient of 90 to 60% organic solvent over 30 min and then 60–0% over 15 min. Fractions were collected every minute at absorbances over 500 mAU and every 5 min otherwise. All fractions were lyophilized prior to LC-MS analysis.

Mass Spectrometry

Dry peptide fractions were resuspended in 0.1% formic acid and loaded onto a Thermo EasyLC. Separate MS/MS analyses were performed for the membrane, cytosolic and glycosylated peptides. The peptides were eluted using a 0–34% organic gradient over 70 min and then 34–100% over 20 min. All LC-MS runs were performed on 75-μm-inner-diameter columns, packed with C18 material (Dr. Maisch, Ammerbuch-Entringen, Germany). Mass spectrometry was performed using higher-energy collisional dissociation (HCD) fragmentation on a Thermo LTQ Velos (Thermo Fisher Scientific, Bremen, Germany). Quantification was performed on reporter tags at m/z 114, 115 and 116. MS settings: a full MS scan in the mass area of 400–1800 Da was performed in the Orbitrap with a resolution of 30,000 FWHM and a target value of 1×10^6 ions. For each full scan, the seven most intense ions (>+1 charge state) were selected for HCD and detected at a resolution of 7500 FWHM. HCD settings: threshold for ion selection was 20,000, the target value of ions used for HCD was 1×10^5, activation time was 1 ms, isolation window was 2.5 Da, and normalized collision energy was 48.0.

All data were searched using Thermo Proteome Discoverer (version 1.3.0.339) and Mascot (v2.2, Matrix Science Ltd., London, UK) allowing for variable methionine oxidation and protein *N*-terminal acetylation. iTRAQ labelling was set as a fixed modification, along with cysteine carbamidomethylation. Enzyme specificity was set for trypsin, with two missed cleavages allowed. Precursor mass tolerance was 10 ppm, and fragment mass tolerance was set to 0.05 Da. Data were searched against a Swiss-Prot rat database (UniProtKB/Swiss-Prot 2012_10). Data were filtered to 1% peptide FDR with a decoy approach using the percolator function in Proteome Discoverer, filtered to remove Mascot scores less than 18 and limited to the best matching peptide for each scan, as described previously (Engholm-Keller et al. 2012). Data were exported from Proteome Discoverer and manually normalized to protein median values across an entire labelling experiment to correct for protein abundance variation. Protein and peptide regulation was defined based on the iTRAQ ratio exceeding two standard deviations from the median ratio for a given tag.

Flow Cytometry

We used flow cytometry for blinded expressional determination of lamininβ2, clathrin heavy chain (HC) and nidogen2 in the VSMCs of the cerebral intraparenchymal vasculature of the forebrain from sham and GCI rats. The hind part of the brain (cerebrum behind MCA and cerebellum) was discarded and the remaining extra-parenchymal vasculature removed from the forebrain structures. The isolation of a single-cell population of the forebrain structures including the intraparenchymal vasculature was performed by a novel technique based on previous protocols, advanced in the our laboratory and described in detail in the following (Navone et al. 2013; van Beijnum et al. 2008). The tissue was disrupted mechanically with a surgical scalpel followed by enzymatic digestion with Liberase TM Research Grade (Roche, Switzerland) for 1.5 h at 37 °C. Red blood cells, granulocytes, non-vital cells and cell debris were removed from the cell suspension by centrifugation on a Ficoll-Paque PLUS (GE Healthcare, Denmark) gradient for 30 min, 400×*g* at room temperature (RT). The interphase of the Ficoll gradient was isolated, leaving us with viable neurons, astrocytes and vascular cells and this cell suspension was fixated in 4% paraformaldehyde for 30 min, then washed with PBS and kept herein until staining and run of experiments.

The single-cell population was permeabilized with 0.25% Triton X-100 PBS (PBS-T, Chemicon, Sweden) for 30 min at RT and incubated in blocking buffer (5% normal donkey serum in PBS) for 2 h at RT. The cell suspensions were stained overnight at 4 °C with primary goat anti-smooth muscle actin 22 (anti-SM22) (1:100, ab10135, Abcam, Cambridge, UK), primary rabbit anti-myosin HC (1:100, myosin HC, ab82541, Abcam), goat isotope control IgG (5 μg/mL, ab37373, Abcam) or rabbit isotype control IgG (5 μg/mL, ab37416, Abcam) in blocking buffer. Subsequently, the cell suspensions were incubated with Alexa Fluor 488-conjugated donkey anti-goat IgG (1:100, 505-545-147, Jackson ImmunoResearch, PA, USA) or allophycocyanin (APC)-conjugated donkey anti-rabbit IgG (1:100, 711-136-152, Jackson ImmunoResearch) for 2 h in the dark at RT.

Next, the cell suspensions were incubated with one of the following primary antibodies: mouse anti-lamininβ2 (1:10, MAB2066, R&D systems, MN, USA), rabbit anti-clathrin

HC (1:100, ab21679, Abcam), goat anti-nidogen2 (1:20, sc-26133, Santa Cruz, USA), mouse isotope control IgG (10 μg/mL, ab18443, Abcam), rabbit isotype control IgG (10 μg/mL, ab37416, Abcam) or goat isotype control IgG (10 μg/mL, ab37373, Abcam) in blocking buffer overnight at 4 °C. Excess primary antibody was removed followed by incubation with DyLight 405-conjugated donkey anti-mouse IgG (1:100, 715-475-150, Jackson ImmunoResearch), APC-conjugated donkey anti-rabbit IgG (1:100, 705-545-147, Jackson ImmunoResearch) or Alexa Fluor 488-conjugated donkey anti-goat IgG (1:100, 705-545-147, Jackson ImmunoResearch) for 2 h in the dark at RT. Finally, excess secondary antibody was removed and the cell suspensions were diluted to a final volume of 0.5 mL with PBS.

The double-stained cell suspensions were analysed by fluorescent-activated cell sorting (FACS) on the BD FACSVerse machine (BD Biosciences, NJ, USA). Fluorescence was induced with a 405-nm violet laser, a 488-nm blue laser and a 640-nm red laser. The single-cell population was defined from the forward scatter versus side scatter plot of all events (supplementary figure; S1 Fig. A and B), and in each experiment for each antibody used, we defined the antibody-specific signal according to the IgG control (supplementary figure; S1 Fig. C–H). Data were analysed by the BD FACSuite Software. The sham and GCI operations, tissue isolation and FACS analyses were performed in pairs, and therefore, results were analysed with Student's two-tailed paired *t* test and $p < 0.05$ was accepted as statistical significant.

Results

Physiological Parameters

For the proteomic screen, we had microvasculature from three groups of rats: GCI + U0126 treatment, GCI + vehicle (DMSO) and sham + vehicle (DMSO). All physiological parameters from the surgeries are presented in Table 1 and were within acceptable physiological limits. Furthermore, there were no significant differences in the physiological parameters when comparing these three groups or with animals operated for validation with flow cytometry (Table 1).

Overview of Experimental Setup and Groups Analysed in the Proteome

The proteomic screen was a tandem mass spectrometry analysis where relative expressional changes were calculated on the basis of iTRAQ labelling. Prior to mass spectrometry, the protein mixture from three to six animals was divided into three fractions analysed separately by mass spectrometry: glycosylated, membrane and cytosolic proteins. A total of 336 glycosylated proteins, 1214 membrane proteins and 405 cytosolic proteins were identified. Upregulated proteins identified in the glycosylated, membrane and cytosolic fractions were pooled into one list, and likewise, downregulated proteins identified in the glycosylated, membrane and cytosolic fractions were pooled into one list for analysis and biological interpretation. We compared the list of proteins upregulated after GCI (vehicle) relative to sham with the list of proteins upregulated after GCI treated with the MEK1/2 inhibitor U0126 relative to sham. We identified 50 proteins for whom the increased expression was found to persist independent of treatment with U0126 (S1 Table) and 82 and 105 proteins that were uniquely upregulated either after vehicle (S3 Table) or U0126 treatment (S5 Table), respectively. Likewise, we compared the list of proteins downregulated after GCI (vehicle) relative to sham with the list of proteins downregulated after GCI treated with U0126 relative to sham. We identified 30 proteins for whom the decreased expression persisted independently of treatment with U0126 (S2 Table) and 42 and 56 proteins that were uniquely downregulated either after vehicle (S4 Table) or U0126 treatment (S6 Table), respectively.

Proteomic Changes in the Cerebral Microvasculature After GCI

A total of 132 proteins were upregulated (Table 2), and 72 proteins were downregulated (Table 3) 72 h after GCI (vehicle) compared to sham. We visualized the proteins that were upregulated and downregulated after GCI separately with STRING (string-db.org, version 10), an online database of known and predicted protein-protein interactions (Szklarczyk et al. 2015).

Proteins Upregulated

STRING revealed a detailed map of known and predicted protein-protein interactions of the proteins found to be upregulated after GCI compared to sham (Fig. 1). Within this map, we identified eight subnetworks (numbered 1–8, Fig. 1) named according to the biological function of the proteins: (1) cellular respiration, (2) structural/cytoskeletal proteins, (3) extracellular matrix (ECM) proteins and fibrinogen, (4) clathrin-mediated endocytosis, (5) ribosomal proteins, (6) chromatin structure-related proteins, (7) myelin-associated proteins and (8) synaptic proteins. Collectively, the network analysis in Fig. 1 illustrated upregulation of proteins involved in the mitochondrial part of cellular respiration (tricarboxylic acid cycle and electron transport chain), clathrin-mediated endocytosis, chromatin structure, ribosomal activity, synaptic activity and myelin composition. Moreover, we found that different structural/cytoskeletal and ECM proteins were upregulated after GCI compared to sham, indicating that a remodelling of the cerebral microvasculature might be taking place.

Table 1 Physiological data from in vivo experiments

	MABP (mmHg) (preischemia)	MABP (mmHg) (during)	MABP (mmHg) (post-ischemia)	pH (preischemia)	pH (post-ischemia)	pCO_2 (kPa)	pO_2 (kPa)	Body temp. (°C)	Cranial temp.(°C)
Sham, $n = 6$ (DMSO)	110.1 ± 12.1	–	–	7.45 ± 0.1	–	3.4 ± 0.3	16.5 ± 0.5	36.9 ± 0.5	37.0 ± 0.5
GCI, $n = 6$ (DMSO)	98.4 ± 10.1	39.3 ± 1.6	116.0 ± 11.0	7.42 ± 0.03	7.35 ± 0.06	4.7 ± 0.6	14.4 ± 1.1	36.8 ± 0.4	37.3 ± 0.4
GCI, $n = 6$ (U0126)	104.3 ± 8.4	41.0 ± 1.6	106.5 ± 20.6	7.45 ± 0.10	7.41 ± 0.11	3.5 ± 1.5	15.3 ± 1.1	36.9 ± 0.3	36.7 ± 0.3
Sham, $n = 672$ h	99.8 ± 13.2	–	–	7.37 ± 0.03	–	4.2 ± 0.6	14.9 ± 2.9	36.9 ± 0.2	37.0 ± 0.2
GCI, $n = 672$ h	92.2 ± 16.3	35.1 ± 1.7	110.5 ± 8.2	7.38 ± 0.04	7.35 ± 0.03	4.4 ± 0.4	15.7 ± 2.4	37.1 ± 0.1	36.9 ± 0.3

Data given as mean ± standard deviation

Proteins Downregulated

The proteins downregulated 72 h after GCI compared to sham were also analysed by STRING, creating a map of protein-protein interactions wherein we identified five subnetworks (numbered 1–5, Fig. 2) named according to the biological function of the proteins: (1) cellular respiration, (2) integrin–collagen interactions, (3) contractile phenotype, (4) G-protein subunits and (5) sodium-potassium pump. Collectively, this network analysis illustrates a downregulation of proteins involved in G-protein-coupled receptor (GPCR) signalling, the contractile phenotype of VSMCs, glycolysis and membrane potential stability.

Proteomic Changes Normalized by Treatment with the MEK1/2 Inhibitor U0126

Next, we identified the microvascular proteins that were regulated after GCI and normalized by treatment with the specific MEK1/2 inhibitor U0126 (Tables 2 and 3). In Table 2, the list of proteins upregulated after GCI is divided into groups representing the subnetworks given in Fig. 1, and within Table 2, it is stated which of the GCI-induced expressional changes that were normalized by the U0126 treatment. We found that at least one of the proteins from each of the eight groups upregulated (Fig. 1) after GCI was normalized in the cerebral microvasculature from GCI rats treated with U0126; however, the U0126 treatment did not normalize the protein expression of all proteins within any of the eight groups upregulated after GCI (Table 2). It is worth highlighting the high levels of normalization which occurs to the structural proteins (5 out of 6 proteins, group 2, Table 2) and proteins involved in clathrin-mediated endocytosis (6 out of 8 proteins, group 4, Table 2); however, the U0126 treatment was found to have little effect on the expressional increase of chromatin-structure related proteins (1 out of 8 proteins normalized, group 6, Table 2). Additionally, the U0126 treatment normalized the upregulation of many non-categorized proteins (Table 2).

In Table 3, the list of proteins downregulated after GCI is divided into groups representing the subnetworks given in Fig. 2, and within Table 3, it is stated which of the GCI-induced expressional changes that were normalized by the U0126 treatment. We found that at least one of the proteins from each of the five groups downregulated after GCI (Fig. 2) was normalized in the cerebral microvasculature from GCI rats treated with U0126 (Table 3). However, post-GCI U0126 treatment had little effect on the expressional decrease of contractile proteins (5 out of 14 normalized, group 3, Table 3) and the protein subunits of the sodium-potassium ATPase (1 out of 3 normalized, group 5, Table 3). Additionally, the U0126 treatment normalized the downregulation of many non-categorized proteins (Table 3).

Verification of Selected Proteins

The increased expression of ECM proteins and proteins involved in clathrin-mediated endocytosis identified in the proteomic screen of the cerebral microvasculature after GCI caught our interest, and we chose to validate the VSMC-specific expression of clathrin HC, lamininβ2 and nidogen2 after GCI and sham operation by flow cytometry.

Flow cytometry analysis revealed that one distinct population of SM22-positive cells (VSMCs) expressed lamininβ2 (upper right quadrant in Fig. 3a, b), and the summary data showed that a significantly increased percentage of VSMCs expressed lamininβ2 after GCI compared to sham ($p = 0.014$, $n = 4$, Fig. 3g). We identified two subpopulations of SM22-positive cells (VSMCs) expressing clathrin HC (upper right quadrant in Fig. 3b), which were both included in the expressional analysis (Fig. 3e). The percentage of SM22-positive cells (VSMCs) expressing clathrin HC tended to increase after GCI compared to sham, although this was not statistically significant ($p = 0.082$, $n = 5$, Fig. 3h). We identified two

Table 2 Proteins upregulated in the cerebral microvasculature 72 h after GCI (vehicle) compared to sham

	Accession number	Protein name	Name in STRING	Peptides	Normalized by U0126
Group 1	P08461	Dihydrolipoyllysine-residue acetyltransferase component of pyruvate dehydrogenase complex, mitochondrial	Dlat	2	Yes
	P42123	L-Lactate dehydrogenase B chain	Ldhb	1	Yes
	Q63362	NADH dehydrogenase [ubiquinone] 1 alpha subcomplex subunit 5	Ndufa5	1	Yes
	O35077	Glycerol-3-phosphate dehydrogenase [NAD(+)], cytoplasmic	Gpd1	1	Yes
	P20070	NADH–cytochrome b5 reductase 3	Cyb5r3	1	Yes
	P97700	Mitochondrial 2-oxoglutarate/malate carrier protein	Slc25a11	1	Yes
	Q6AXV4	Sorting and assembly machinery component 50 homolog	Samm50	4	Yes
	Q4QQV3	Protein FAM162A	Fam162a	1	Yes
	B0K020	CDGSH iron–sulphur domain-containing protein 1	Cisd1	6	Yes
	Q5XIN6	LETM1 and EF-hand domain-containing protein 1, mitochondrial	Letm1	2	Yes
	P04166	Cytochrome b5 type B	Cyb5b	5	–
	P05708	Hexokinase-1	Hk1	1	–
	P15999	ATP synthase subunit alpha, mitochondrial	Atp5a1	2	–
	O54715	V-type proton ATPase subunit S1	Atp6ap1	1	–
	P10719	ATP synthase subunit beta, mitochondrial	Atp5b	1	–
	Q99NA5	Isocitrate dehydrogenase [NAD] subunit alpha, mitochondrial	Idh3a	1	–
	Q05962	ADP/ATP translocase 1	Slc25a4	7	–
	Q3KR86	Mitochondrial inner membrane protein (fragment)	Immt	1	–
	Q9Z2L0	Voltage-dependent anion-selective channel protein 1	Vdac1	1	–
	P81155	Voltage-dependent anion-selective channel protein 2	Vdac2	3	–
	P62815	V-type proton ATPase subunit B, brain isoform	Atp6v1b2	1	–
Group 2	P31000	Vimentin	Vim	1	Yes
	Q63862	Myosin-11 (fragments)	Myh11	3	Yes
	Q63355	Unconventional myosin-Ic	Myo1c	1	Yes
	P28023	Dynactin subunit 1	Dctn1	1	Yes
	P62738	Actin, aortic smooth muscle	Acta2	2	Yes
	Q5XIF6	Tubulin alpha-4A chain	Tuba4a	1	–
Group 3	B5DFC9	Nidogen2	Nid2	1	Yes
	P15800	Laminin subunit beta	Lamb2	2	Yes
	Q9EQP5	Prolargin	Prelp	2	Yes
	P47853	Biglycan	Bgn	1	Yes
	P06399	Fibrinogen alpha chain	Fga	6	Yes
	P02680	Fibrinogen gamma chain	Fgg	16	Yes
	Q68VK5	Tetraspanin-5	Tspan5	1	Yes
	P16086	Spectrin alpha chain, non-erythrocytic 1	Sptan1	1	Yes
	Q9EPF2	Cell surface glycoprotein MUC18	Mcam	1	Yes
	P32736	Opioid-binding protein/cell adhesion molecule	Opcml	2	Yes
	Q1WIM3	Cell adhesion molecule 3	Cadm3	2	Yes
	P14480	Fibrinogen beta chain	Fgb	1	–
	O35112	CD166 antigen	Alcam	7	–
	O88775	Embigin	Emb	6	–
	Q99P82	Claudin-11	Cldn11	2	–
	P13852	Major prion protein	Prnp	1	–
	P01830	Thy-1 membrane glycoprotein	Thy1	3	–
	P49134	Integrin beta-1	Itgb1	1	–
Group 4	P84092	AP-2 complex subunit mu	Ap2m1	1	Yes
	P62744	AP-2 complex subunit sigma	Ap2s1	2	Yes
	P62944	AP-2 complex subunit beta	Ap2b1	1	Yes
	O55012	Phosphatidylinositol-binding clathrin assembly protein	Picalm	1	Yes
	Q07647	Solute carrier family 2, facilitated glucose transporter member 3	Slc2a3	2	Yes
	Q4V8H8	EH domain-containing protein 2	Ehd2	1	Yes
	P11442	Clathrin heavy chain 1	Cltc	1	–
	P61206	ADP-ribosylation factor 3	Arf3	1	–
Group 5	P19804	Nucleoside diphosphate kinase B	Nme2	1	Yes
	P41123	60S ribosomal protein L13	Rpl13	1	Yes
	P62909	40S ribosomal protein S3	Rps3	1	Yes
	P62271	40S ribosomal protein S18	Rps18	1	Yes
	P62912	60S ribosomal protein L32	ENSRNOG00000032605	1	Yes
	P49242	40S ribosomal protein S3a	Rps3a	6	–
	P27952	40S ribosomal protein S2	Rps2	1	–
	P21533	60S ribosomal protein L6	Rpl6	1	–
Group 6	Q00715	Histone H2B type 1	H2b	9	Yes

Table 2 (continued)

	Accession number	Protein name	Name in STRING	Peptides	Normalized by U0126
	P84245	Histone H3.3	H3f3b	2	–
	A9UMV8	Histone H2A.J	ENSRNOG00000033045	6	–
	P15865	Histone H1.4	Hist1h1d	2	–
	P0C0S7	Histone H2A.Z	H2afz	2	–
	Q6P747	Heterochromatin protein 1-binding protein 3	Hp1bp3	3	–
	Q02874	Core histone macro-H2A.1	H2afy	1	–
	P62804	Histone H4	Hist2h4	6	–
Group 7	P07722	Myelin-associated glycoprotein	Mag	3	Yes
	P02688	Myelin basic protein	Mbp	1	Yes
	Q812E9	Neuronal membrane glycoprotein M6-a	Gpm6a	1	Yes
	Q0ZHH6	Atlastin-3	Atl3	1	Yes
	Q64548	Reticulon-1	Rtn1	1	Yes
	P60203	Myelin proteolipid protein	Plp1	22	–
	Q63345	Myelin-oligodendrocyte glycoprotein	Mog	2	–
Group 8	Q02563	Synaptic vesicle glycoprotein 2A	Sv2a	8	Yes
	P60905	DnaJ homolog subfamily C member 5	Dnajc5	6	Yes
	P61265	Syntaxin-1B	Stx1b	1	Yes
	P21707	Synaptotagmin-1	Syt1	2	Yes
	P61765	Syntaxin-binding protein 1	Stxbp1	1	–
	P07825	Synaptophysin	Syp	1	–
	P19491	Glutamate receptor 2	Gria2	1	–
	Q9JI12	Vesicular glutamate transporter 2	Slc17a6	1	–
Non-categorized	P07340	Sodium/potassium-transporting ATPase subunit beta-1	Atp1b1	1	Yes
	P11506	Plasma membrane calcium-transporting ATPase 2	Atp2b2	1	Yes
	P48037	Annexin A6	Anxa6	2	Yes
	P25122	Potassium voltage-gated channel subfamily C member 1	Kcnc1	1	Yes
	P46101	Dipeptidyl aminopeptidase-like protein 6	Dpp6	2	Yes
	P25099	Adenosine receptor A1	Adora1	1	Yes
	O09175	Aminopeptidase B	Rnpep	1	Yes
	P47752	Sphingosine 1-phosphate receptor 2	S1pr2	1	Yes
	Q80ZA5	Sodium-driven chloride bicarbonate exchanger	Slc4a10	2	Yes
	Q9WVR6	Large neutral amino acids transporter small subunit 2	Slc7a8	1	Yes
	Q9Z1E1	Flotillin-1	Flot1	2	Yes
	P31662	Sodium-dependent neutral amino acid transporter SLC6A17	Slc6a17	4	Yes
	P33124	Long-chain-fatty-acid–CoA ligase 6	Acsl6	1	Yes
	P70580	Membrane-associated progesterone receptor component 1	Pgrmc1	2	Yes
	P07687	Epoxide hydrolase 1	Ephx1	1	Yes
	Q6AXM8	Serum paraoxonase/arylesterase 2	Pon2	1	Yes
	P36365	Dimethylaniline monooxygenase [*N*-oxide-forming] 1	Fmo1	2	Yes
	P47819	Glial fibrillary acidic protein	Gfap	3	Yes
	Q9JJW1	Tetraspanin-2	Tspan2	1	Yes
	Q07936	Annexin A2	Anxa2	2	Yes
	Q5FVI4	Cell cycle exit and neuronal differentiation protein 1	Cend1	1	Yes
	P97546	Neuroplastin	Nptn	2	Yes
	P14668	Annexin A5	Anxa5	4	Yes
	P07936	Neuromodulin	Gap43	1	Yes
	Q80U96	Exportin-1	Xpo1	1	Yes
	Q9WVC0	Septin-7	sep–07	1	Yes
	P97536	Cullin-associated NEDD8-dissociated protein 1	Cand1	2	Yes
	P97710	Tyrosine-protein phosphatase non-receptor type substrate 1	Sirpa	1	Yes
	P12346	Serotransferrin	Tf	1	Yes
	O08590	Membrane primary amine oxidase	Aoc3	7	Yes
	P46462	Transitional endoplasmic reticulum ATPase	Vcp	1	Yes
	Q6AXX6	Redox-regulatory protein FAM213A	RGD1309676	2	Yes
	Q9EQT5	Tubulointerstitial nephritis antigen-like	Tinagl1	1	Yes
	P00762	Anionic trypsin-1	Prss1	6	–
	P05371	Clusterin	Clu	1	–
	P10252	CD48 antigen	Cd48	1	–
	P11654	Nuclear pore membrane glycoprotein 210	Nup210	1	–
	P13596	Neural cell adhesion molecule 1	Ncam1	5	–
	P14740	Dipeptidyl peptidase 4	Dpp4	2	–
	P18418	Calreticulin	Calr	1	–
	P19643	Amine oxidase	Maob	2	–

Table 2 (continued)

Accession number	Protein name	Name in STRING	Peptides	Normalized by U0126
P23785	Granulins	Grn	1	–
P25235	Dolichyl-diphosphooligosaccharide–protein glycosyltransferase subunit 2	Rpn2	1	–
Q5I0E7	Transmembrane emp24 domain-containing protein 9	Tmed9	2	–
Q63081	Protein disulphide-isomerase A6	Pdia6	1	–
Q64428	Trifunctional enzyme subunit alpha, mitochondrial	Hadha	1	–
Q80Z70	Protein sel-1 homolog 1	Sel1l	1	–
Q9WVK7	Hydroxyacyl-coenzyme A dehydrogenase, mitochondrial	Hadh	1	–

Proteins are divided into groups according to the subnetworks identified in Fig. 1. Accession number, protein name and name in STRING are given, along with the number of upregulated peptides; each protein identification was based upon and whether post-GCI treatment with the MEK1/2 inhibitor U0126 normalized the expression of a given protein

subpopulations of myosin HC-positive cells (VSMCs) expressing nidogen2 (upper right quadrant in Fig. 3c), which were both included in the expressional analysis (Fig. 3f). The percentage of VSMCs expressing nidogen2 was significantly increased after GCI compared to sham ($p = 0.026$, $n = 5$, Fig. 3i).

Discussion

This is the first study to generate a proteomic in-depth characterization of the cerebral microvascular proteins regulated after GCI and how treatment with the MEK1/2 inhibitor U0126 normalized several of these expressional changes. The possible functional consequences of the upregulated and downregulated subnetworks of expressional changes identified in Figs. 1 and 2 are discussed by dividing the important GCI-induced cerebral microvascular changes into nine main categories. Within each of the nine categories, the effect of the U0126 treatment on the GCI-induced expressional changes is discussed (Tables 2 and 3). The nine categories of GCI-induced expressional changes are: 1. Altered cellular respiration, 2. Remodelling of the ECM, 3. Decreased contractile phenotype, 4. Increased clathrin-mediated endocytosis, 5. Increased expression of chromatin structure-related protein, 6. Increased ribosomal protein expression, 7. Increased synaptic activity, 8. Altered G-protein signalling and 9. Instability of the membrane potential.

1. Altered cellular respiration: we found a decreased expression of glycolytic enzymes and an increased expression of citric acid cycle enzymes and mitochondrial proteins involved in adenosine triphosphate (ATP) production and L-lactate dehydrogenase. This indicates decreased glycolysis activity and increased lactate metabolism and mitochondrial production of ATP in the cerebral microvasculature after GCI. However, we also found a decreased expression of a few mitochondrial proteins involved in ATP production. Treatment with U0126 normalized the GCI-induced decrease in glycolytic enzymes and mitochondrial proteins and the GCI-induced increase of L-lactate dehydrogenase, whereas the U0126 treatment only partly normalized the expressional increase of citric acid cycle enzymes and proteins involved in mitochondrial ATP production. Collectively, this indicates that the U0126 treatment partly normalizes the GCI-induced altered cellular respiration of the cerebral microvascular cells. The effect of the U0126 treatment on lactate metabolism might also be a secondary effect as increased lactate metabolism has been shown to correlate with cerebral ischemic damage (Dienel 2014).
2. Remodelling of the ECM: we found increased expression of the extracellular proteins nidogen2, prolargin, lamininβ2 and biglycan and a decreased expression of collagen type I (α1 and α2 chain) and integrins α7, β1 and β4. The expressions of integrin and ECM proteins were normalized by the U0126 treatment, whereas the expression of collagen type I was downregulated both in vehicle- and in U0126-treated animals. We also found increased expression of fibrinogen after GCI, which was partly normalized by the U0126 treatment (2 out of 3 proteins normalized). Interestingly, fibrinogen has previously been shown to deposit in the microvascular wall after cerebral ischemia (Baeten and Akassoglou 2011).

Remodelling of the ECM may decrease the elasticity of the cerebral intraparenchymal arterioles, and such pathological arterial stiffness is thought to be involved in various cerebrovascular disorders (Martinez-Lemus et al. 2009a), and therefore, these expressional changes caught our interest. Extracellular proteins are produced and secreted from VSMCs, endothelial cells and perivascular astrocytes, and we find that the percentage of VSMCs expressing lamininβ2 and nidogen2 increased 72 h after GCI (Fig. 3). Nidogen2 is an ECM protein primarily found in the basement membrane between the endothelial cells and VSMCs (Ho et al. 2008),

Table 3 Proteins downregulated in the cerebral microvasculature 72 h after GCI compared to sham

	Accession number	Protein name	Name in STRING	Peptides	Normalized by U0126
Group 1	P04797	Glyceraldehyde-3-phosphate dehydrogenase	Gapdh	1	Yes
	P19511	ATP synthase F(0) complex subunit B1, mitochondrial	Atp5f1	1	Yes
	P05065	Fructose-bisphosphate aldolase A	Aldoa	3	Yes
	P05708	Hexokinase-1	Hk1	2	Yes
	Q641Y2	NADH dehydrogenase [ubiquinone] iron–sulphur protein 2, mitochondrial	Ndufs2	1	Yes
	P48500	Triosephosphate isomerase	ENSRNOG00000015290	1	Yes
	Q5RJQ4	NAD-dependent protein deacetylase sirtuin-2	Sirt2	1	Yes
	P16036	Phosphate carrier protein, mitochondrial	Slc25a3	1	Yes
	P01946	Haemoglobin subunit alpha-1/2	Hba2	2	Yes
	Q66HD0	Endoplasmin	Hsp90b1	2	Yes
	P15429	Beta-enolase	Eno3	1	Yes
	P11240	Cytochrome c oxidase subunit 5A, mitochondrial	Cox5a	2	Yes
	P13635	Ceruloplasmin	Cp	1	Yes
	Q794F9	4F2 cell surface antigen heavy chain	Slc3a2	3	–
Group 2	Q63258	Integrin alpha-7	Itga7	1	Yes
	P49134	Integrin beta-1	Itgb1	5	Yes
	Q64632	Integrin beta-4	Itgb4	1	Yes
	P02454	Collagen alpha-1(I) chain	Col1a1	39	–
	P02466	Collagen alpha-2(I) chain	Col1a2	3	–
	Q9Z1P2	Alpha-actinin-1	Actn1	1	–
Group 3	P02564	Myosin-7	Myh7	12	Yes
	Q29RW1	Myosin-4	Myh4	3	Yes
	P12847	Myosin-3	Myh3	1	Yes
	Q63610	Tropomyosin alpha-3 chain	Tpm3	2	Yes
	P58775	Tropomyosin beta chain	Tpm2	5	Yes
	P02563	Myosin-6	Myh6	2	–
	P02600	Myosin light chain 1/3, skeletal muscle isoform	Myl1	1	–
	P04462	Myosin-8 (fragment)	Myh1	1	–
	P08733	Myosin regulatory light chain 2, ventricular/cardiac muscle isoform	Myl2	2	–
	P13413	Troponin I, slow skeletal muscle	Tnni1	2	–
	P16409	Myosin light chain 3	Myl3	2	–
	P68136	Actin, alpha skeletal muscle	Acta1	8	–
	P00564	Creatine kinase M-type	Ckm	7	–
	P11507	Sarcoplasmic/endoplasmic reticulum calcium ATPase 2	Atp2a2	3	–
Group 4	P54311	Guanine nucleotide-binding protein G(I)/G(S)/G(T) subunit beta-1	Gnb1	2	Yes
	P04897	Guanine nucleotide-binding protein G(i) subunit alpha-2	Gnai2	1	Yes
	P10824	Guanine nucleotide-binding protein G(i) subunit alpha-1	Gnai3	2	–
Group 5	P06686	Sodium/potassium-transporting ATPase subunit alpha-2	Atp1a2	10	Yes
	P06685	Sodium/potassium-transporting ATPase subunit alpha-1	Atp1a1	1	–
	P07340	Sodium/potassium-transporting ATPase subunit beta-1	Atp1b1	11	–
Non-categorized	P97710	Tyrosine-protein phosphatase non-receptor type substrate 1	Sirpa	1	Yes
	P70627	Glutamate carboxypeptidase 2	Folh1	1	Yes
	Q63633	Solute carrier family 12 member 5	Slc12a5	1	Yes
	P31596	Excitatory amino acid transporter 2	Slc1a2	3	Yes
	P47942	Dihydropyrimidinase-related protein 2	Dpysl2	1	Yes
	Q9JI66	Electrogenic sodium bicarbonate cotransporter 1	Slc4a4	1	Yes

Table 3 (continued)

Accession number	Protein name	Name in STRING	Peptides	Normalized by U0126
P48284	Carbonic anhydrase 4	Car4	1	Yes
P25286	V-type proton ATPase 116 kDa subunit a isoform 1	Atp6v0a1	1	Yes
P54290	Voltage-dependent calcium channel subunit alpha-2/delta-1	Cacna2d1	2	Yes
P67779	Prohibitin	Phb	1	Yes
P02688	Myelin basic protein	Mbp	1	Yes
Q3SWT0	Platelet endothelial cell adhesion molecule	Pecam1	2	Yes
P58195	Phospholipid scramblase 1	Plscr1	2	Yes
Q920Q0	Paralemmin-1	Palm	4	Yes
P27615	Lysosome membrane protein 2	Scarb2	1	Yes
Q9QWE9	Gamma-glutamyltransferase 5		2	Yes
Q9WTQ2	Podocalyxin	Podxl	2	Yes
P0C5X8	Protein tweety homolog 1	Ttyh1	1	Yes
P61265	Syntaxin-1B	Stx1b	1	–
P70560	Collagen alpha-1(XII) chain (fragment)		1	–
Q29RW1	Myosin-4	Myh4	2	–
Q62745	CD81 antigen	Cd81	2	–
Q63135	Complement component receptor 1-like protein	Cr1l	2	–
Q63564	Synaptic vesicle glycoprotein 2B	Sv2b	1	–
Q924C3	Ectonucleotide pyrophosphatase/phosphodiesterase family member 1	Enpp1	2	–
P07153	Dolichyl-diphosphooligosaccharide–protein glycosyltransferase subunit 1	Rpn1	1	–
D3ZFB6	Proline-rich transmembrane protein 2	Prrt2	1	–
P11167	Solute carrier family 2, facilitated glucose transporter member 1	Slc2a1	1	–
P14562	Lysosome-associated membrane glycoprotein 1	Lamp1	1	–
P14669	Annexin A3	Anxa3	2	–
P15589	Steryl-sulphatase	Sts	1	–
P15684	Aminopeptidase N	Anpep	16	–
P21396	Amine oxidase [flavin-containing] A	Maoa	1	–

Proteins are divided into groups according to the subnetworks identified in Fig. 2. Accession number, protein name and name in STRING are given, along with the number of downregulated peptides; each protein identification was based upon and if post-GCI treatment with the MEK1/2 inhibitor U0126 normalized the expression of the protein

and genetic ablation of nidogen2 in mice has been shown to increase vessel wall permeability in the lung (Mokkapati et al. 2012). The increased expression of ECM proteins and decreased expression of integrins indicate thickening of the extracellular basement membrane and its detachment from the surrounding cells, which might compromise the intraparenchymal vascular function since the proximity of astrocytes and vascular cells is important for normal vascular function (del Zoppo 2009). In support, a previous study showed thickening of the vascular basement membrane 24 h after GCI (Wisniewski et al. 1995). Furthermore, the expression of extracellular proteins was previously shown to increase in the cerebral microvasculature 24 h after GCI in rat (Haqqani et al. 2005).

Collectively, the results of the proteomic screen and verification of a GCI-induced increased percentage of VSMCs expressing the ECM proteins lamininβ2 and nidogen2 support the hypothesis of ECM remodelling in the cerebral microvasculature after GCI. We speculate that ECM remodelling results in altered microvascular function contributing to delayed neuronal damage after GCI.

3. Decreased contractile phenotype: we found a decreased expression of different isoforms of tropomyosin, myosin and muscle-specific actin. Additionally, we found an increased expression of cytoskeletal proteins like actin, vimentin and myosin isoforms involved in intracellular movement. The U0126 treatment had minor effects on

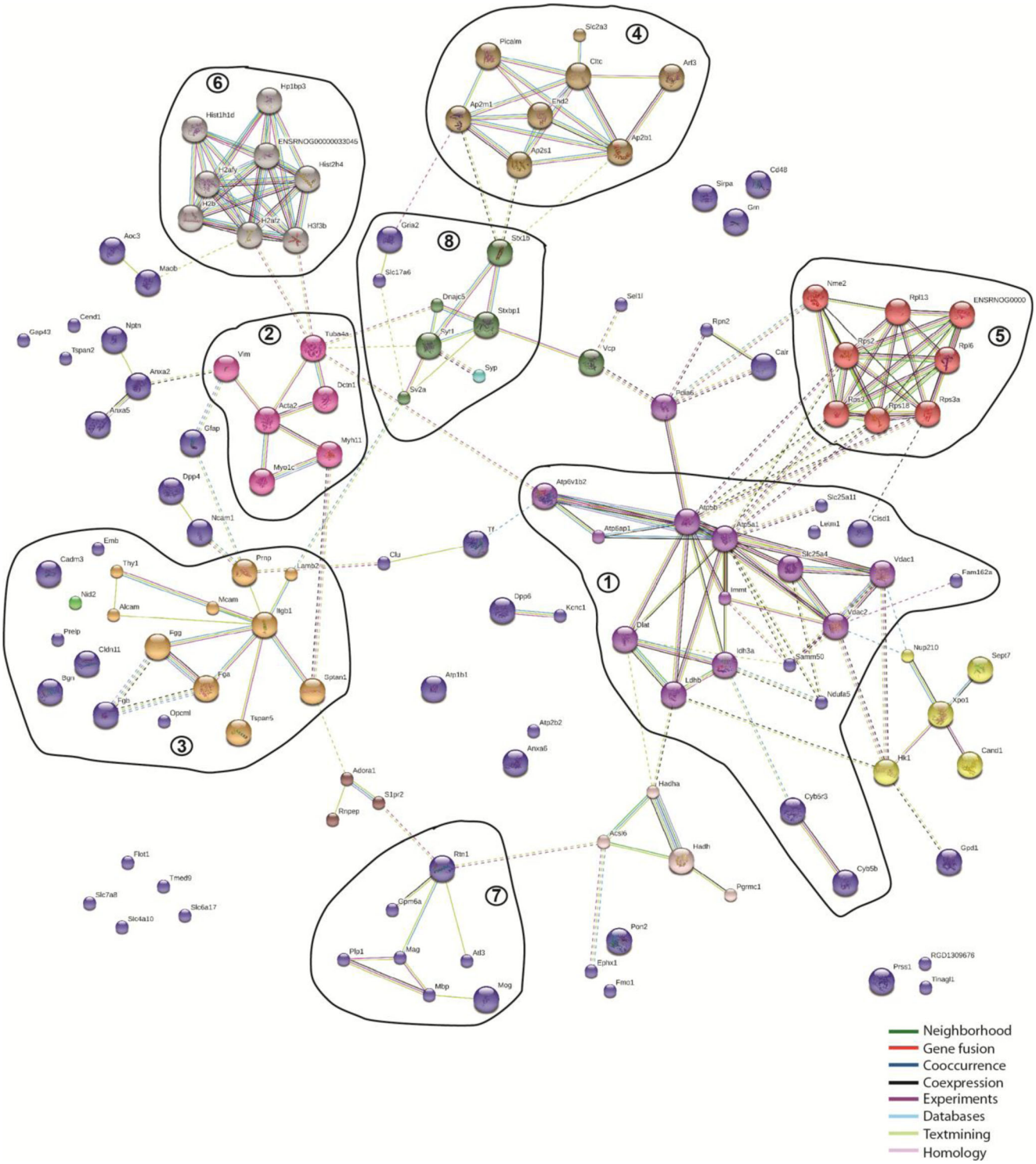

Fig. 1 Protein interactions of proteins upregulated 72 h after GCI (vehicle) compared to sham. Protein interactions were analysed by STRING, and within the overall network, we depicted eight subnetworks, numbered *1–8* in the figure: (*1*) cellular respiration, (*2*) structural/cytoskeletal proteins, (*3*) fibrinogen–extracellular matrix (ECM) interactions, (*4*) clathrin-mediated endocytosis, (*5*) ribosomal proteins, (*6*) expression of chromatin structure-related proteins, (*7*) myelin-associated proteins and (*8*) synaptic proteins. See Table 2 for a complete list of the proteins in the network. A known and strong prediction of a protein-protein interaction is marked by a *solid line*, whereas a *dashed line* indicates a weak protein-protein interaction. The protein-protein interactions are colour coded based on the nature of the protein-protein interaction and the colour index given in the figure. STRING, version 10, string-db.org (Szklarczyk et al. 2015)

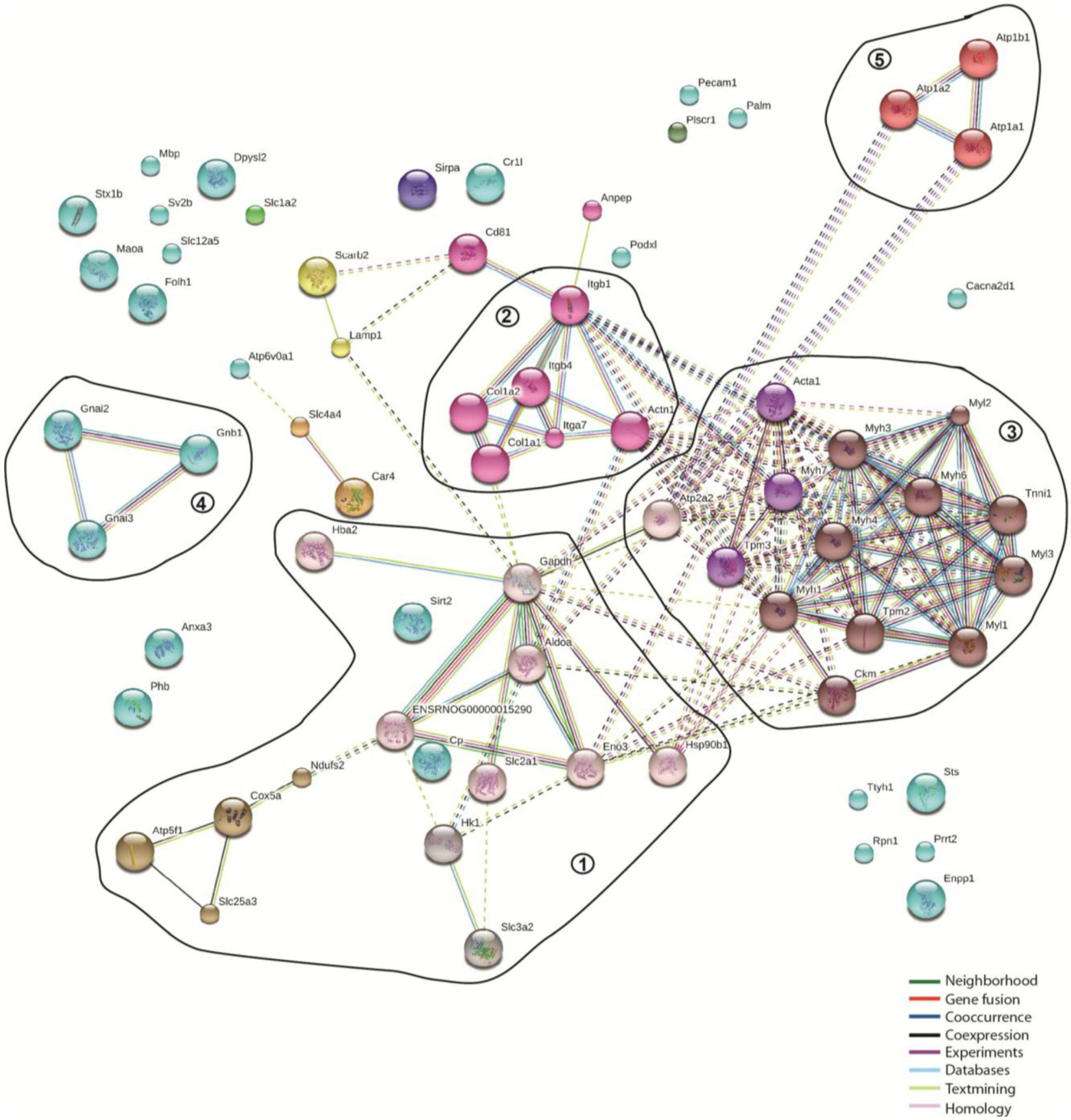

Fig. 2 Protein interactions of proteins downregulated 72 h after GCI (vehicle) compared to sham. Protein interactions were analysed by STRING, and within the overall network generated, we depicted five subnetwork numbered *1–5* in the figure: (*1*) cellular respiration, (*2*) integrin–collagen interactions, (*3*) contractile phenotype, (*4*) G-protein subunits and (*5*) sodium-potassium pump. See Table 3 for a complete list of the proteins in the network. A known and strong prediction of a protein-protein interaction is marked by a *solid line*, whereas a *dashed line* indicates a weak protein-protein interaction. The protein-protein interactions are colour coded based on the nature of the protein-protein interaction and the colour index given in the figure. STRING, version 10, string-db.org (Szklarczyk et al. 2015)

the expressional decrease of contractile protein expression (5 out of the 14 normalized, Table 3) after GCI.

We hypothesize that the decreased contractile phenotype identified by expressional changes in the proteome reflected initial phenotypic switching of VSMCs in the cerebral microvasculature. Phenotypic changes of the VSMCs in different pathologies like atherosclerosis, hypertension and diabetes are a widely recognized phenomenon, where the VSMCs transform from a specialized contractile phenotype to a non-

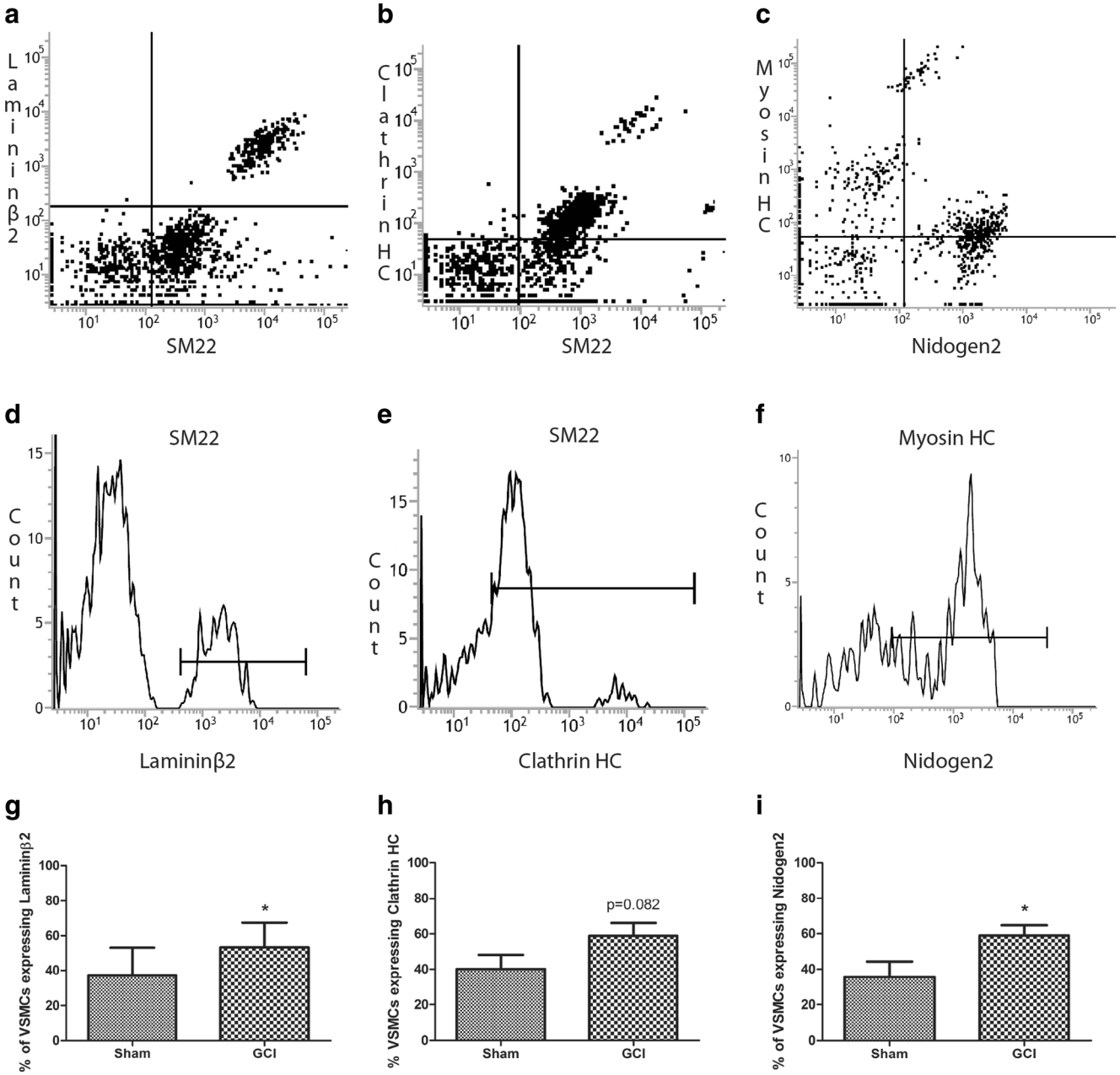

Fig. 3 VSMC-specific expression and verification of expressional upregulation of laminin β2, clathrin HC and nidogen2 by flow cytometry. Single-cell populations were stained with antibodies for the protein of interest (laminin β2, clathrin HC and nidogen2) and antibodies for detection of VSMCs (SM22 or myosin HC). In the single-cell populations, we detect one population expressing laminin β2 (**a**) and one major and one minor population of cells expressing clathrin HC (**b**) and nidogen2 (**c**). The percentage of VSMCs expressing laminin β2, clathrin HC or nidogen2 was determined in the VSMC-specific gate (SM22 or myosin HC) according to the histograms (**d**–**f**). The summary data showed a significantly increased percentage of VSMCs expressing laminin β2 (**g**, $n = 4$) and nidogen2 (**i**, $n = 5$) after GCI compared to sham. The percentage of VSMCs expressing clathrin HC tended to increase after GCI compared to sham but was not significant (**h**, $n = 5$). Data presented as mean ± SEM, and statistical significance was evaluated by two-tailed, paired Student's t test, $^*p < 0.05$

contractile, proliferative phenotype (Martinez-Lemus et al. 2009b). As found in the proteome, increased expression of vimentin (cytoskeletal protein) and decreased expression of collagen type I α1 have been shown to occur in cultured VSMC stimulated to undergo a phenotypic switch (Rocchiccioli et al. 2012). Furthermore, biglycan expression was increased 72 h after GCI, and interestingly, VSMC-specific overexpression of biglycan in mice was previously shown to increase vascular hypertrophy and proliferation, indicating that the composition of ECM proteins can contribute to the induction of a phenotypic switch in VSMCs (Shimizu-Hirota et al. 2004).

4. Clathrin-mediated endocytosis: the expression of proteins involved in clathrin-mediated endocytosis increased in the cerebral microvasculature after GCI (vehicle) compared to sham and was normalized by treatment with U0126, except for the expression of clathrin HC. With flow cytometry, we found a tendency towards an increased percentage of VSMCs expressing clathrin HC in the cerebral microvasculature 72 h after GCI ($n = 5$, $p = 0.082$). Increased expression of proteins associated with clathrin-mediated endocytosis might indicate increased activity of this mechanism after GCI compared to sham. Clathrin-mediated endocytosis is primarily involved in constitutive and stimulated internalization of receptors (McMahon and Boucrot 2011), and thereby, clathrin-mediated endocytosis regulates the cellular processes initiated by these receptors.
5. Increased ribosomal protein expression: we found an increased expression of several ribosomal proteins in the cerebral microvasculature after GCI (vehicle) compared to sham, which might indicate increased ribosomal activity and, thereby, increased translational activity. The GCI-induced expressional increase in 4 out of 7 ribosomal proteins was normalized when post-GCI treatment with the MEK1/2 inhibitor U0126 was applied.
6. Increased expression of chromatin structure-related proteins: the increased expression of several histone isoforms and other chromatin-related proteins in the cerebral microvasculature after GCI (vehicle) was not normalized by treatment with the MEK1/2 inhibitor U0126, expect for the expression of histone H2B type 1. Histone isoform composition in the nucleosome and altered expression of histone isoforms can change epigenetic control of the DNA and thereby alter gene expression (Findeisen et al. 2013; Zhu et al. 2008), and we hypothesize that the increased expression of several histone isoforms might indicate changes in the epigenetic control and, thereby, the gene expression of the microvascular cells. Furthermore, epigenetic mechanisms are known to contribute to the phenotypic shift of VSMC (Findeisen et al. 2013; Liu et al. 2015), and we hypothesize that the decreased contractile phenotype of the cerebral microvasculature identified in the proteomic screen (point 3 above) might be early indications of a phenotypic switch of the VSMCs.
7. Increased synaptic activity: the expression of several proteins involved in synaptic activity increased after GCI, which might point to an increased activity of neurons in close contact with the cerebral microvasculature and thereby affect the microvascular function in vivo. The increased expression of proteins involved in synaptic activity was partly reversed by the U0126 treatment.
8. Altered G-protein signalling: we found that a decreased expression of the G-protein subunits β1, α inhibitory 2 (αi2) and α inhibitory 3 (αi3) in the cerebral microvasculature after GCI compared to sham and U0126 treatment partly normalized these expressional changes (2 out of 3 proteins normalized, Table 3). Changes in G-protein subunit expression might affect GPCR-mediated signalling coupled to these G-proteins. Adenylate cyclase is inactivated by αi2 and αi3, and therefore, adenylate cyclase activity might be increased due to expressional downregulation of αi2 and αi3. Ion channels can be activated by the βγ-complex and thereby alter the membrane potential of the cell and, therefore, the contractile state of VSMCs; thus, the decreased expression of β1 might indicate decreased ion channel activity (Dascal 2001; Edvinsson and Krause 2002).
9. Instability in the membrane potential: we found a decreased expression of sodium-potassium ATPase subunits α1, α2 and β1 after GCI compared to sham which partly persisted in U0126-treated GCI rats (group 5, Table 3). A decreased activity of the sodium-potassium ATPase points to an increased membrane potential and, thereby, increased cellular vulnerability of the microvascular cells after GCI. In support, sodium-potassium ATPase activity was previously shown to be decreased after cerebral ischemia (Yang et al. 1992).

Conclusion

In summary, this proteomic screen provides insight into the expressional changes of the cerebral microvasculature after GCI compared to sham and which of these expressional changes that might be normalized when treatment with the MEK1/2 inhibitor U0126 was applied in GCI rats. Proteomics is a strong tool to utilize when evaluating the overall effect of new treatments, especially when testing a broad kinase inhibitor such as the MEK1/2 inhibitor U0126. The proteomic data point to many different expressional changes induced by GCI that can be prevented by early U0126 treatment; however, it is still unclear which of these effects are beneficial and which are detrimental. Previous treatment candidates for delayed cerebral ischemic damage were primarily neuroprotective and/or focused on individual downstream targets, whereas our view is that this cannot work because several different pathological pathways are transcribed and translated after GCI. We have previously shown that MEK1/2 signalling causes transcription of a large number of vascular proteins such as contractile receptors, proinflammatory molecules and metalloproteinases in the extra-parenchymal arteries after cerebral ischemia, which we termed vascular plasticity (Edvinsson and Povlsen 2011). This study illustrates that GCI induces multiple diverse expressional changes in the cerebral intraparenchymal vasculature in addition to the changes of the extra-parenchymal large arteries.

Moreover, the effect of GCI on the intraparenchymal vasculature is broad and complex and can most likely only be effectively prevented by broad transcriptional inhibition such as obtained by targeting the MEK1/2 pathway.

Acknowledgements We kindly acknowledge the Lundbeck Foundation for financial support (LE—Grant of Excellence and MRL—Junior Group Leader Fellowship).

References

Attwell D, Buchan AM, Charpak S, Lauritzen M, Macvicar BA, Newman EA (2010) Glial and neuronal control of brain blood flow. Nature 468:232–243

Baeten KM, Akassoglou K (2011) Extracellular matrix and matrix receptors in blood-brain barrier formation and stroke. Dev Neurobiol 71: 1018–1039

Bradbury MW (1993) The blood-brain barrier. Exp Physiol 78:453–472

Dascal N (2001) Ion-channel regulation by G proteins. Trends Endocrinol Metab 12:391–398

del Zoppo GJ (2009) Relationship of neurovascular elements to neuron injury during ischemia. Cerebrovasc Dis 27(Suppl 1):65–76

Dienel GA (2014) Lactate shuttling and lactate use as fuel after traumatic brain injury: metabolic considerations. J Cereb Blood Flow Metab 34:1736–1748

Edvinsson L, Krause DN (2002) Cerebral blood flow and metabolism. Lippincott Williams and Wilkins

Edvinsson LI, Povlsen GK (2011) Vascular plasticity in cerebrovascular disorders. J Cereb Blood Flow Metab 31:1554–1571

Engholm-Keller K, Birck P, Storling J, Pociot F, Mandrup-Poulsen T, Larsen MR (2012) TiSH—a robust and sensitive global phosphoproteomics strategy employing a combination of TiO2, SIMAC, and HILIC. J Proteome 75:5749–5761

Findeisen HM, Kahles FK, Bruemmer D (2013) Epigenetic regulation of vascular smooth muscle cell function in atherosclerosis. Curr Atheroscler Rep 15:319.

Haqqani AS, Nesic M, Preston E, Baumann E, Kelly J, Stanimirovic D (2005) Characterization of vascular protein expression patterns in cerebral ischemia/reperfusion using laser capture microdissection and ICAT-nanoLC-MS/MS. FASEB J 19:1809–1821

Ho MS, Bose K, Mokkapati S, Nischt R, Smyth N (2008) Nidogens—extracellular matrix linker molecules. Microsc Res Tech 71:387–395

Johansson S, Povlsen GK, Edvinsson L (2012) Expressional changes in cerebrovascular receptors after experimental transient forebrain ischemia. PLoS One 7:e41852

Johansson SE, Larsen SS, Povlsen GK, Edvinsson L (2014) Early MEK1/2 inhibition after global cerebral ischemia in rats reduces brain damage and improves outcome by preventing delayed vasoconstrictor receptor upregulation. PLoS One 9:e92417

Johansson SE, Andersen XE, Hansen RH, Povlsen GK, Edvinsson L (2015) Cerebrovascular endothelin-1 hyper-reactivity is associated with transient receptor potential canonical channels 1 and 6 activation and delayed cerebral hypoperfusion after forebrain ischaemia in rats. Acta Physiol (Oxf) 214:376–389

Liu R, Leslie KL, Martin KA (2015) Epigenetic regulation of smooth muscle cell plasticity. Biochim Biophys Acta 1849:448–453

Martinez-Lemus LA, Hill MA, Meininger GA (2009a) The plastic nature of the vascular wall: a continuum of remodeling events contributing to control of arteriolar diameter and structure. Physiology (Bethesda) 24:45–57

Martinez-Lemus LA, Hill MA, Meininger GA (2009b) The plastic nature of the vascular wall: a continuum of remodeling events contributing to control of arteriolar diameter and structure. Physiology (Bethesda) 24:45–57

McMahon HT, Boucrot E (2011) Molecular mechanism and physiological functions of clathrin-mediated endocytosis. Nat Rev Mol Cell Biol 12:517–533

Mokkapati S, Bechtel M, Reibetanz M, Miosge N, Nischt R (2012) Absence of the basement membrane component nidogen 2, but not of nidogen 1, results in increased lung metastasis in mice. J Histochem Cytochem 60:280–289

Navone SE, Marfia G, Invernici G, Cristini S, Nava S, Balbi S, Sangiorgi S, Ciusani E, Bosutti A, Alessandri G, Slevin M, Parati EA (2013) Isolation and expansion of human and mouse brain microvascular endothelial cells. Nat Protoc 8:1680–1693

Neumann JT, Cohan CH, Dave KR, Wright CB, Perez-Pinzon MA (2013) Global cerebral ischemia: synaptic and cognitive dysfunction. Curr Drug Targets 14:20–35

Pardridge WM, Yang J, Eisenberg J, Tourtellotte WW (1987) Isolation of intact capillaries and capillary plasma membranes from frozen human brain. J Neurosci Res 18:352–357

Petito CK, Feldmann E, Pulsinelli WA, Plum F (1987) Delayed hippocampal damage in humans following cardiorespiratory arrest. Neurology 37:1281–1286

Pulsinelli WA, Brierley JB, Plum F (1982) Temporal profile of neuronal damage in a model of transient forebrain ischemia. Ann Neurol 11: 491–498

Rocchiccioli S, Ucciferri N, Comelli L, Trivella MG, Citti L, Cecchettini A (2012) Proteomics changes in adhesion molecules: a driving force for vascular smooth muscle cell phenotypic switch. Mol BioSyst 8: 1052–1059

Shimizu-Hirota R, Sasamura H, Kuroda M, Kobayashi E, Hayashi M, Saruta T (2004) Extracellular matrix glycoprotein biglycan enhances vascular smooth muscle cell proliferation and migration. Circ Res 94:1067–1074

Smith ML, Bendek G, Dahlgren N, Rosen I, Wieloch T, Siesjo BK (1984) Models for studying long-term recovery following forebrain ischemia in the rat. 2. A 2-vessel occlusion model. Acta Neurol Scand 69: 385–401

Steen H, Mann M (2004) The ABC's (and XYZ's) of peptide sequencing. Nat Rev Mol Cell Biol 5:699–711

Szklarczyk D, Franceschini A, Wyder S, Forslund K, Heller D, Huerta-Cepas J, Simonovic M, Roth A, Santos A, Tsafou KP, Kuhn M, Bork P, Jensen LJ, von Mering C (2015) STRING v10: protein-protein interaction networks, integrated over the tree of life. Nucleic Acids Res 43:D447–D452

van Beijnum JR, Rousch M, Castermans K, van der Linden E, Griffioen AW (2008) Isolation of endothelial cells from fresh tissues. Nat Protoc 3:1085–1091

Wisniewski HM, Pluta R, Lossinsky AS, Mossakowski MJ (1995) Ultrastructural studies of cerebral vascular spasm after cardiac arrest-related global cerebral ischemia in rats. Acta Neuropathol 90:432–440

Yang GY, Chen SF, Kinouchi H, Chan PH, Weinstein PR (1992) Edema, cation content, and ATPase activity after middle cerebral artery occlusion in rats. Stroke 23:1331–1336

Zeng YS, Xu ZC (2000) Co-existence of necrosis and apoptosis in rat hippocampus following transient forebrain ischemia. Neurosci Res 37:113–125

Zhu Z, Boobis AR, Edwards RJ (2008) Identification of estrogen-responsive proteins in MCF-7 human breast cancer cells using label-free quantitative proteomics. Proteomics 8:1987–2005